Food Chemistry 433 (2024) 137266

Contents lists available at ScienceDirect

Food Chemistry

journal homepage: www.elsevier.com/locate/foodchem

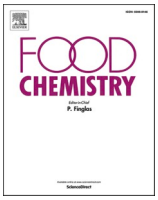

Mechanistic kinetic modelling of lipid oxidation in vegetable oils to estimate shelf-life

Khoa A. Nguyen [a], Marie Hennebelle [a], John P.M. van Duynhoven [b,c], Arend Dubbelboer [d], Vincent J.P. Boerkamp [a], Peter A. Wierenga [a,*]

[a] Wageningen University & Research, Laboratory of Food Chemistry, Bornse Weilanden 9, 6708 WG Wageningen, The Netherlands
[b] Unilever Food Innovation Centre, Bronland 14, 6708 WH Wageningen, The Netherlands
[c] Wageningen University & Research, Laboratory of Biophysics, Stippeneng 4, 6708 WE Wageningen, The Netherlands
[d] Danone Nutricia Research, Uppsalalaan 12, 3584 CT Utrecht, The Netherlands

ARTICLE INFO

Keywords:
Lipid oxidation
Vegetable oils
Modelling kinetic reactions
Shelf-life tests
Second oxidation phase

ABSTRACT

Estimating the shelf-life of vegetable oils is important to develop solutions to reduce spoilage by lipid oxidation. Typically, the shelf-life is predicted by detecting secondary oxidation markers in accelerated shelf-life tests, which are time-consuming. Existing numerical approaches using early primary oxidation products as predictive markers do not account for variations in fatty acid types, antioxidants, or storage conditions. A mechanistic kinetic model was developed incorporating these factors as a step towards shelf-life prediction for vegetable oils. Specific kinetic constants for the reactions of each unsaturated fatty acid type account for variations in fatty acid composition, and oxygen mass transfer accounts for variations in oxygen conditions. A second acceleration of lipid oxidation observed in long-term storage experiments was described by a multiplication factor for the kinetic constants related to oxidation products. Our model accurately extrapolates short-time experimental data to estimate long term formation of oxidation products under the same conditions.

1. Introduction

Estimating the shelf-life of vegetable oils is of great interest for food industries. The shelf-life of such products is compromised by lipid oxidation, which leads to the formation of off-flavours and odors as well as a decrease in nutritional value. Lipid oxidation is a radical chain reaction that can be delayed by the presence of antioxidants (AH), such as tocopherols, and catalysed by pro-oxidants (e.g., ferrous Fe^{2+} and ferric Fe^{3+} ions). It is commonly divided into two phases: primary and secondary oxidation (Schaich, 2020). Primary oxidation is initiated by the formation of lipid radicals ($L^{\bullet}$) from an unsaturated fatty acid (LH). These $L^{\bullet}$ react quickly with O_2 to form peroxyl radicals ($LOO^{\bullet}$). The latter reacts further with another LH to form new alkyl radicals ($L^{\bullet}$) that can propagate the reaction, and hydroperoxides (LOOHs), also described as the primary oxidation products. Termination of the radical chain reaction occurs when two radicals react with each other to form non-radical products. Finally, during secondary oxidation, LOOHs are degraded further into aldehydes (ADs), epoxides (EPs), and other secondary oxidation products, which include volatile compounds that are responsible for the off-flavours and odors.

The shelf-life of a product is limited due to these off-flavour/odor compounds, which can take months to evolve and be detected under consumer-relevant conditions. Accelerated shelf-life tests at elevated temperatures are commonly used to assess oxidative stability of raw materials and products during product development or within the supply chain. Although accelerated tests reduce the time required to determine the shelf-life, they still take weeks to months to detect the formation of secondary oxidation products causing off-flavours/odors (Syed, 2016). In such tests and for the later text in this manuscript, the maximum shelf-life is defined as the time at which the secondary oxidation products begin to increase significantly (i.e., the onset time). This shelf-life definition has been used more commonly in other literature on lipid oxidation in accelerated shelf-life tests (Boerkamp et al., 2022; Merkx et al., 2021). For temperatures up to 40 °C, modelling approaches could use primary oxidation products (hydroperoxides) to predict the onset of secondary oxidation products (e.g., off-flavours) of oils at the same conditions, and thereby estimate the shelf-life (Laguerre et al., 2020b). At higher temperatures, the fast decomposition of LOOHs

* Corresponding author.
E-mail address: peter.wierenga@wur.nl (P.A. Wierenga).

https://doi.org/10.1016/j.foodchem.2023.137266
Received 3 March 2023; Received in revised form 15 July 2023; Accepted 22 August 2023
Available online 26 August 2023

precludes use of LOOHs as predictive markers to estimate the onset of secondary oxidation products (Faubion et al., 2022).

A number of mathematical modelling methods have been designed to simulate the formation of the primary oxidation product (LOOHs) in different food systems (i.e., foods, oils, and emulsions). For instance, analytical approximations have been used to describe the accumulation of total LOOHs in oils (Farhoosh, 2022; Farhoosh, 2021; Li et al., 2020; Patsioura et al., 2017) and foods (Özilgen and Özilgen, 1990) where the first acceleration phase follows sigmoidal behaviour until reaching a plateau. This sigmoidal production of LOOHs has been described by mathematical equations, e.g., Gompertz, Foubert, and logistic functions, as were applied to oxidation in emulsions (Farhoosh, 2022; Farhoosh, 2021; Li et al., 2020; Merkx et al., 2021; Patsioura et al., 2017; Wardhani et al., 2013).

Experimental observations typically show three stages of LOOH formation (Farhoosh, 2022; Laguerre et al., 2020a; Merkx et al., 2021; Patsioura et al., 2017): an initial lag phase, an exponential increase phase, then a decline in rate until a steady state is almost reached (Fig. S1A). In other studies, two sigmoidal curves were observed instead of one (Boerkamp et al., 2022; Chen et al., 2012; Merkx et al., 2021); after the first sigmoidal curve, the kinetic rate of LOOH formation increases again in what is referred to as the second acceleration phase (Fig. S1B1). It has been suggested that this second acceleration phase begins at a specific concentration of LOOH, the critical concentration of LOOHs or $C_{LOOH,\ critical}$ that coincides with the onset of secondary oxidation products (Fig. S1B2) (Merkx et al., 2021). The absence of this second acceleration phase in some datasets can be attributed to the two following reasons. First, larger or scattered intervals were used between sampling time points, thus data points required to observe the transition to the second acceleration phase were not available (as illustrated in Fig. S2). Second, the shelf-life duration used was too short to observe the second acceleration phase, and so the onset of secondary oxidation products (Hoppenreijs et al., 2021; Merkx et al., 2021) (Fig. S1B1 and B2).

While the mechanism behind the second acceleration phase and the function of the critical LOOH concentration is not well understood, the concept of oxidation acceleration and onset of secondary product generation when total LOOH concentration reaches a threshold value can provide a useful target in modelling. The depletion of antioxidants or the presence of metal ions does not seem to be responsible for the second acceleration phase. However, they do play an important role on the induction period and therefore, on the time required to reach the $C_{LOOH,\ critical}$ (Chen et al., 2012).

Typically, existing models do not account for oil composition and storage conditions (Li et al., 2020; Patsioura et al., 2017; Wardhani et al., 2013). Some models also estimate long term LOOH formation up to the $C_{LOOH,critical}$ by extrapolating data collected during early oxidation (Merkx et al., 2021). However, none of these approaches capture the full complexity of lipid oxidation. To obtain a model that integrates mechanism with kinetics, more explicit parameters are needed. First, models typically did not explicitly include reaction constants for reactions of individual fatty acid (e.g., with 1, 2, or 3 double bonds). It is, however, known that the kinetic constant of LOOH formation is lower for monounsaturated fatty acids (e.g., C18:1n-9) than for polyunsaturated fatty acids because C-H bonds are dissociated more readily between two double bonds than next to only one double bond (Schaich, 2020). Existing models do not account for such fatty acid specific reactions, and therefore lack flexibility in predicting the shelf-life of vegetable oils with different fatty acid compositions. Second, the existing models often neglect O_2 mass transfer, despite the fact that O_2 plays a key role in the lipid oxidation (Johnson and Decker, 2015; Laguerre et al., 2017). This makes it difficult to predict oxidation in systems with different oil/headspace volumes, or different initial O_2 partial pressures. Third, secondary oxidation products formed in the second acceleration phase are responsible for off-flavours and therefore limit shelf life. It is therefore essential to include the second acceleration phase to model the full extent of lipid oxidation reactions. Finally, a complete mechanistic kinetic model that accounts for the three aspects described above requires the estimation of many model parameters in order to be used for predictions, thus simultaneously fitting O_2 headspace profile, primary oxidation products (individual LOOHs), and secondary oxidation products (total aldehydes and epoxides) is required.

The development of a mechanistic kinetic model was reported here for lipid oxidation that can be used to estimate shelf-life of oils with different oil composition under different O_2 conditions. The modelling of lipid oxidation in vegetable oils involved assigning specific kinetic constants to the reactions of different types of unsaturated fatty acids, accounting for O_2 mass transfer, and determining acceleration factors when the $C_{LOOH,\ critical}$ was reached. To estimate the model parameters, the predicted formation of oxidation products by the model was fitted to experimental data (of O_2 in headspace, LOOHs, aldehydes, and epoxides) using a multi-response optimization. Then, the predictive performance of the kinetic model was evaluated for oxidation of oils varying in

Table 1
Overview of lipid oxidation reactions as they can occur in vegetable oils. The terms 'k' are the kinetic constants of the respective reactions.

1. Primary lipid oxidation reactions		
Initiation	$LH \xrightarrow{k_i} L^\bullet + H^\bullet$	(R1)
Formation of hydroperoxides	$L^\bullet + O_2 \xrightarrow{k_{p1}} LOO^\bullet$	(R2)
	$LOO^\bullet + LH \xrightarrow{k_{p2}} LOOH + L^\bullet$	(R3)
2. Secondary oxidation reactions		
Degradation of hydroperoxides	$LOOH \xrightarrow{k_d} LO^\bullet + OH^\bullet$	(R4)
	$OH^\bullet + LH \xrightarrow{k_{p3}} L^\bullet + H_2O$	(R5)
Formation of aldehydes	$LO^\bullet + LH \xrightarrow{k_s} AD + L^\bullet$	(R6)*
Formation of epoxides	$LO^\bullet \xrightarrow{k_{e1}} EP^\bullet$	(R7)
	$EP^\bullet + LH \xrightarrow{k_{e2}} EP + L^\bullet$	(R8)**
	$EP^\bullet + O_2 \xrightarrow{k_{e3}} EPOO^\bullet$	(R9)
	$EPOO^\bullet + LH \xrightarrow{k_{e4}} EPOOH + L^\bullet$	(R10)
3. Inhibition, catalysis and termination		
Antioxidant	$LOO^\bullet + AH \xrightarrow{k_{AH1}} LOOH + A^\bullet$	(R11)
	$LO^\bullet + AH \xrightarrow{k_{AH2}} LOH + A^\bullet$	(R12)
	$L^\bullet + AH \xrightarrow{k_{AH3}} LH + A^\bullet$	(R13)
Redox cycle (pro-oxidation)	$LOOH + Fe^{3+} \xrightarrow{k_{pro1}} LOO^\bullet + H^+ + Fe^{2+}$ slow	(R14)
	$LOOH + Fe^{2+} \xrightarrow{k_{pro2}} LO^\bullet + OH^- + Fe^{3+}$ fast	(R15)
Termination	$L^\bullet + L^\bullet \xrightarrow{k_{t1}}$ non-radical products	(R16)
	$L^\bullet + LOO^\bullet \xrightarrow{k_{t2}}$ non-radical products	(R17)
	$LOO^\bullet + LOO^\bullet \xrightarrow{k_{t3}}$ non-radical products + O_2	(R18)
	$LOO^\bullet + A^\bullet \xrightarrow{k_{t4}}$ non-radical products	(R19)
	$A^\bullet + A^\bullet \xrightarrow{k_{t5}}$ non-radical products	(R20)

Abbreviations: $EP^\bullet$, epoxy alkyl radical, $EPOO^\bullet$, epoxy peroxyl radical, EPOOH, hydroperoxyl epoxide and $A^\bullet$, antioxidant radical.

* R6 results from the combination of $R^\bullet + LH \rightarrow RH + L^\bullet$ (H abstraction) and $LO^\bullet \rightarrow AD + R^\bullet$ (homolytic beta scission).

** R8 is commonly expected to be much slower than R9, but was included in the model since experimental data showed the significant formation of monoepoxides (EP).

the initial fatty acid composition, amount of antioxidants, and initial O_2 partial pressures. Finally, our model was tested for its ability to use short-time experimental data to estimate lipid oxidation during longer time storage under the same conditions, with the goal of reducing experimental time required for shelf-life testing, thereby, increasing the rate of development for new ingredients, anti-oxidants, and approaches for achieving a desired shelf-life.

2. Material and methods

2.1. Datasets

The datasets originated from two previous shelf-life studies where lipid oxidation products and headspace O_2 partial pressure profiles were measured. In brief, the first dataset was acquired by incubating 1 mL non-stripped rapeseed oil in a 20.4 mL ND18 headspace vials (type 548-0248A) with screw caps with a 1.3 mm PTFE septum (type 548-0822A, VWR international, the Netherlands). Experiments were performed either in open or closed vials, resulting in that O_2 partial pressure in the headspace was constant at 21%, or declining from initial 21% at initial time points, respectively (Boerkamp et al., 2022). Incubation temperatures of 20 and 40 °C were chosen to eliminate possible changes in oxidation mechanisms at higher temperatures (Syed, 2016). In the second dataset, 56 mL conventional rapeseed oils (CRSO), sunflower oils (SFO), and high-oleic sunflower oils (HOSFO) with tocopherols were incubated at 40 °C in a 112 mL polypropylene containers (Securibox with snap caps, Joma Packaging, Austria) under initial 21% O_2 headspace in closed vials. All shelf-life experiments were conducted in the dark without agitation.

These datasets were divided between training and test datasets, summarized in Table S1. The training dataset contained data from non-stripped rapeseed oil oxidized under initial 21% O_2 headspace in closed vials (Boerkamp et al., 2022) was used to estimate the kinetic constants, the acceleration factors, and the $C_{LOOH,\ critical}$. The test dataset contained four separate datasets, i.e., from non-stripped rapeseed oil in open vials, and from the conventional rapeseed, sunflower, and high-oleic sunflower oils in closed vials as described above. The model was run using the kinetic constants obtained after optimising the training datasets, and only changing inputs on initial oil composition. The outcome of the model was compared to the test datasets to evaluate the ability of model predictions.

2.2. Analyses

O_2 partial pressure in the headspace was monitored with a MOCON OpTech-O_2 oxygen sensor (Ametek Mocon, Brooklyn Park, MN, USA) using procedures of Boerkamp et al. (2022). Hydroperoxides and aldehydes were quantified in duplicate by ^{1}H NMR (relative standard deviation $\leq$ 25%), and epoxides were quantified in duplicate by ^{1}H–^{13}C HSQC NMR (relative standard deviation $\leq$ 11.6%). The limit of detection (LOD) for lipid hydroperoxides and aldehydes was 0.01 mmol/kg oil (Merkx et al., 2018). The LOD for the quantification of epoxides by HSQC NMR was 0.19 mmol/kg oil (Boerkamp et al., 2022). For the hydroperoxides, both total hydroperoxides, as well as hydroperoxides derived from specific unsaturated fatty acids (i.e., C18:1n-9, C18:2n-6, and C18:3n-3) were quantified using the ^{1}H NMR as previously described in Merkx et al. (2018).

2.3. Lipid oxidation reactions in vegetable oils

The reactions used in this model are listed in Table 1, i.e., primary lipid oxidation (R1-R3), secondary oxidation (R4-R10), inhibition (R11-R13), catalysis (R14-R15), and termination (R16-R20) reactions. These reactions describe the loss of reactants and formation of oxidation products as observed in experiments. Extension of the model to real food systems will require consideration of other compounds that also may participate in these reactions.

2.4. Mechanistic kinetic model of the lipid oxidation reactions

2.4.1. Model assumptions

The following assumptions were made for the development of the mechanistic kinetic model (1) The O_2, radicals, and oxidation products were assumed to be uniformly distributed in the oil and headspace, i.e., O_2 diffusion is fast compared to time scale of the experiment so at each time point, there is no O_2 gradient as a function of the oil height; (2) As reported in literature, the kinetic constant of Fe^{3+} (k_{pro1}, Table 1) was assumed to be 100 times lower than the kinetic constant of Fe^{2+} (k_{pro2}, Table 1) during the redox cycle of iron ions (R14-15, Table 1). Thus, in the model, the kinetic constant for Fe^{2+} was treated as a fitting parameter, while the constant for Fe^{3+} was calculated as 1/100 of the Fe^{2+} constant; (3) Observations in both training and test datasets showed that the critical LOOH concentration ($C_{LOOH,critical}$) was similar in all different vegetable oils included in this study, and was thus assumed to be constant in the model when applied to oils.

2.4.2. Model construction

2.4.2.1. Governing equations for the accumulation of oxidation products. The kinetic rates (in mol.m^{-3}.s^{-1}) of the 3 main oxidation products (i.e., LOOH, AD, and EPs) were the sum of the kinetic rates of the relevant underlying reactions in Table 1:

$$\frac{d[\mathbf{LOOH}]}{dt} = \mathbf{r}_3 + \mathbf{r}_{11} + \mathbf{r}_4 + \mathbf{r}_{14} + \mathbf{r}_{15} \quad (1)$$

$$\frac{d[\mathbf{AD}]}{dt} = \mathbf{r}_6 \quad (2)$$

$$\frac{d[\mathbf{EPs}]}{dt} = \mathbf{r}_{7,8} + \mathbf{r}_{7,9,10} \quad (3)$$

where [**LOOH**] and [**AD**] embody the concentrations of LOOH and AD, respectively, while [**EPs**] embodies the sum of epoxide (R8) and hydroperoxyl epoxide (R10) concentrations.

The concentrations (i.e., [**LOOH**], [**AD**], and [**EPs**]) were expressed in bold as vectors from different fatty acids. For instance, the vector [**LOOH**] = ([LOOH(1)], [LOOH(2)], [LOOH(3)]) indicates the vector of the concentrations of LOOHs originating from fatty acids with 1-, 2- and 3- double bonds, respectively. In this study, we focused only on oleic (C18:1n-9), linoleic (C18:2n-6), and alpha-linolenic (C18:3n-3) acids, as they are the most abundant unsaturated fatty acids in our oils.

The kinetic rates (**r**) were obtained by describing the chemical reactions (in Table 1) as the first order reaction (for R1, R4, and R7) and the second order reaction for the remaining reactions (van Boekel, 2008):

$$\mathbf{r}_3 = \mathbf{k}_{p2}[\mathbf{LOO^\bullet}][LH] = \left(k_{p2}(1)[LOO^\bullet(1)] + k_{p2}(2)[LOO^\bullet(2)] + k_{p2}(3)[LOO^\bullet(3)]\right)[LH] \quad (4)$$

where [LH] = [LH(1)] + [LH(2)] + [LH(3)].

$$\mathbf{r}_4 = -\mathbf{k}_d[\mathbf{LOOH}] \quad (5)$$

$$\mathbf{r}_6 = \mathbf{k}_a[\mathbf{LO^\bullet}][\mathrm{LH}] \quad (6)$$

$$\mathbf{r}_{7,8} = \mathbf{k}_{e1}\mathbf{k}_{e2}[\mathbf{LO^\bullet}][\mathrm{LH}] \quad (7)$$

$$\mathbf{r}_{7,9,10} = \mathbf{k}_{e1}\mathbf{k}_{e3}\mathbf{k}_{e4}[\mathbf{LO^\bullet}]\left[O_{2,BO}\right][\mathrm{LH}] \quad (8)$$

$$\mathbf{r}_{11} = \mathbf{k}_{AH1}[\mathbf{LOO^\bullet}][\mathrm{AH}] \quad (9)$$

$$\mathbf{r}_{14} = -\mathbf{k}_{pro1}[\mathbf{LOOH}][Fe^{3+}] \quad (10)$$

$$\mathbf{r}_{15} = -\mathbf{k}_{pro2}[\mathbf{LOOH}][Fe^{2+}] \quad (11)$$

where $\mathbf{k}$ = (k(1), k(2), k(3)) embodies a vector of kinetic constants k (in $m^3.mol^{-1}.s^{-1}$), with one entry for each type of fatty acid. This was done to account for the fact that each unsaturated fatty acid oxidizes via the same reactions (Table 1), but with different kinetic constants (Schaich, 2020; Schneider et al., 2008). Similarly, [$\mathbf{LOO^\bullet}$] and [$\mathbf{LO^\bullet}$] are the vectors of the concentrations of $LOO^\bullet$ and $LO^\bullet$ respectively, while [Fe^{3+}], [Fe^{2+}], [AH], and [$O_{2,BO}$] are the scalar concentrations of Fe^{3+}, Fe^{2+}, antioxidants, and the O_2 concentration in the bulk oil (section 2.4.2.2), respectively.

2.4.2.2. Governing equations of O_2 mass transfers. Two O_2 mass transfer processes were considered, one through the cap (O_2 permeability and/or leakage) and the other at the headspace-oil surface (Fig. S3). The concentrations over time of O_2 in the headspace and in the oil are described by the following kinetic rates (in $m^3.mol^{-1}.s^{-1}$):

$$\frac{d[O_{2,HS}]}{dt} = \frac{1}{V_{HS}}\left(\varphi_{O_2}^{Pe} + \varphi_{O_2}^{S}\right) \quad (12)$$

$$\frac{d[O_{2,BO}]}{dt} = -\frac{1}{V_{BO}}\left(\varphi_{O_2}^{S} + \varphi_{O_2}^{BO}\right) \quad (13)$$

where $\varphi_{O_2}^{Pe}$, $\varphi_{O_2}^{S}$, and $\varphi_{O_2}^{BO}$ (in $mol.s^{-1}$) are the kinetic rate of the change in O_2 concentration in the oil phase, through the cap, and at the oil-headspace surface, respectively; V_{HS} and V_{BO} (in m^3) designate the volume of headspace and of the oil phase, respectively.

To describe the governing equations of the kinetic rates, we combined Fick's first law with Henry's law (Chaix et al., 2015). First, $\varphi_{O_2}^{BO}$ (in $mol.s^{-1}$) is the kinetic rate of the change in O_2 concentration in the oil phase (calculated by Eq.15), which was estimated using reactions R2, R9 and R18 in Table 1.

Second, the O_2 permeability/leakage $\varphi_{O_2}^{Pe}$ (in $mol.s^{-1}$), which reflects the change in O_2 concentration between the headspace and the external atmosphere over time, was expressed as:

$$\varphi_{O_2}^{Pe} = k_{Pe}\left(p_{O_2,\infty} - p_{O_2,HS}\right) \quad (14)$$

where k_{Pe} (in $mol.s^{-1}.Pa^{-1}$) is the O_2 permeability/leakage coefficient, $p_{O_2,\infty}$ and $p_{O_2,HS}$ (in Pa) are the O_2 partial pressure in the external atmosphere and the headspace, respectively.

Finally, the O_2 solubilization φ_{O2}^{S} (in $mol.s^{-1}$), which reflects the exchange of O_2 between the headspace and the oil over time, was expressed as:

$$\varphi_{O_2}^{S} = k_{O_2}\frac{A_I}{RT}\left(p_{O_2,HS,S} - p_{O_2,HS}\right) \quad (15)$$

where A_I denotes the headspace-oil surface area (m^2), R (8.314 $J.mol^{-1}.K^{-1}$) is the ideal gas constant, T (in K) is the storage temperature. Also, k_{O_2} (in $m.s^{-1}$) is the O_2 mass transfer coefficient at the headspace-oil surface (Cuvelier et al., 2017; Takahashi et al., 2001) and was calculated as follows:

$$k_{O_2} = \frac{BiD_{O_2}}{L_c} \quad (16)$$

where Bi (dimensionless) is the Biot number (10^5), D_{O_2} (0.93×10^{-9} in $m^2.s^{-1}$ at 20 °C) is the O_2 apparent diffusivity in the oil (Pénicaud et al., 2010), and L_c (in m) is a characteristic length. $p_{O2,HS,I}$ (in Pa) is the O_2 partial pressure at the headspace-oil surface, calculated based on the following equation:

$$p_{O_2,HS,I} = \frac{[O_{2,S}]}{k_{H,O_2}} \quad (17)$$

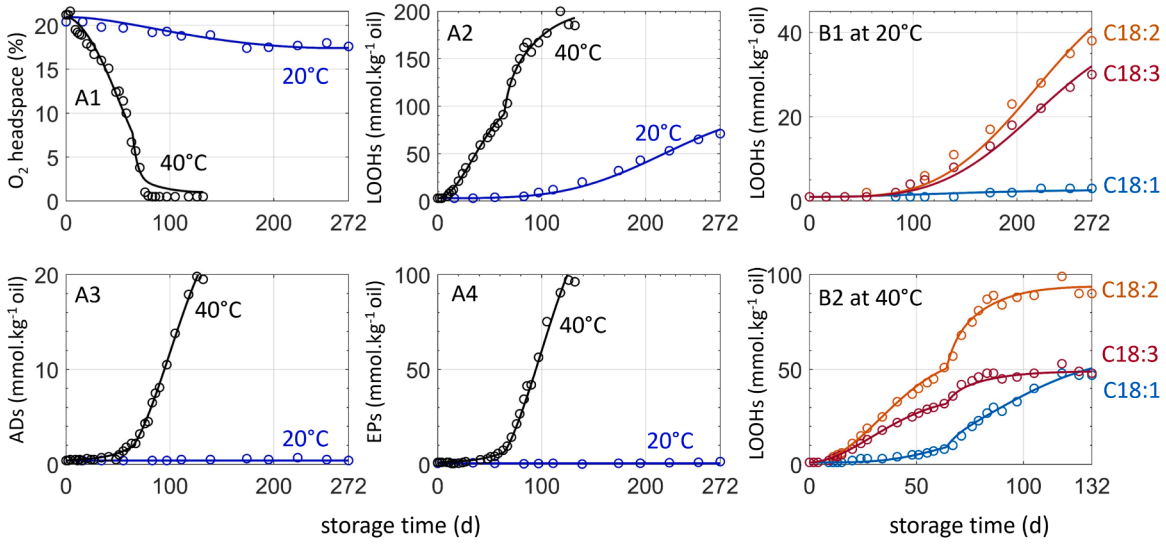

Fig. 1. Fit of numerical (lines) and experimental profiles (open circles, training datasets 1 and 2 in Table S1) at 20 °C (dark blue) and 40 °C (black). (A1) O_2 in the headspace, (A2) total LOOHs, (A3) total ADs and (A4) total EPs in oils; (B) LOOHs (labelled and coloured) formed from C18:1n-9, C18:2n-6, and C18:3n-3. Note that the scale of the y axis between the sub-figures is not similar. (For interpretation of the references to colour in this figure legend, the reader is referred to the web version of this article.)

Table 2
Values of the model parameters **k** and **f** at 20 and 40 °C, estimated from the final model versus reported in the literature.

Parameters* ($mol^{-1}.m^3.s^{-1}$)	20 °C				40 °C			
	# double bonds			Literature value	# double bonds			Literature value#
	1	2	3		1	2	3	
Kinetic constants of primary oxidation reactions								
$\mathbf{k}_i$	1.1×10^{-29}	1.1×10^{-29}	1.1×10^{-29}	–	7.3×10^{-28}	3×10^{-14}	6.9×10^{-13}	10^{-15a}
$\mathbf{k}_{p1}$	34 ($\mathbf{f}_{p1}$ = 3.4)	29 ($\mathbf{f}_{p1}$ = 12.2)	32.5 ($\mathbf{f}_{p1}$ = 12.6)	–	1.5×10^{3} ($\mathbf{f}_{p1}$ = 1.7)	55 ($\mathbf{f}_{p1}$ = 6.1)	500 ($\mathbf{f}_{p1}$ = 6.3)	~10^2 at 37°C[b]
$\mathbf{k}_{p2}$	7.8×10^{-6} ($\mathbf{f}_{p2}$ = 29.3)	0.002 ($\mathbf{f}_{p2}$ = 15)	0.0025 ($\mathbf{f}_{p2}$ = 10.8)	–	3.1×10^{-5} ($\mathbf{f}_{p2}$ = 2.9)	1.2×10^{-3} ($\mathbf{f}_{p2}$ = 1.5)	1.6×10^{-4} ($\mathbf{f}_{p2}$ = 1.08)	3×10^{-4} to 10^{-3a}
Kinetic constants of secondary oxidation reactions								
$\mathbf{k}_d$	3.3×10^{-14}	3.3×10^{-14}	3.3×10^{-14}	–	9.3×10^{-11}	8.3×10^{-13}	3.3×10^{-13}	1.7×10^{-9a}
$\mathbf{k}_a$	9×10^{-5} ($\mathbf{f}_{ka}$ = 10)	4×10^{-4} ($\mathbf{f}_{ka}$ = 50)	2.8×10^{-4} ($\mathbf{f}_{ka}$ = 10)	3.3×10^{-5}, 0.03[c]	0.31 ($\mathbf{f}_{ka}$ = 1.9)	0.1 ($\mathbf{f}_{ka}$ = 9.2)	0.1 ($\mathbf{f}_{ka}$ = 6.09)	–
$\mathbf{k}_{EP}$**	10^{-3} ($\mathbf{f}_{kEP}$ = 50)	10^{-3} ($\mathbf{f}_{kEP}$ = 70)	10^{-3} ($\mathbf{f}_{kEP}$ = 50)	0.032 to 3.3[c]	0.85 ($\mathbf{f}_{kEP}$ = 3.4)	4.3 ($\mathbf{f}_{kEP}$ = 3.5)	0.1($\mathbf{f}_{kEP}$ = 43.7)	–
$\mathbf{k}_{EPOOH}$**	10^{-13}	10^{-13}	10^{-13}	–	10^{-13}	10^{-13}	10^{-13}	–
Kinetic constants of inhibition and catalysis reactions								
$\mathbf{k}_{pro2}$	5×10^{-13}	8.3×10^{-13}	3.3×10^{-12}	–	5×10^{-13}	5×10^{-13}	5×10^{-13}	–
$\mathbf{k}_{AH1}$	8×10^{-3}	8.2×10^{-3}	8×10^{-3}	–	2.5×10^{-2}	8.2×10^{-3}	8×10^{-3}	–
$\mathbf{k}_{AH2}$	1.03×10^{-2}	8.5×10^{-3}	8.6×10^{-3}	–	1.7×10^{-2}	8.5×10^{-3}	8.4×10^{-3}	–

* The kinetic constants were estimated at the specified temperatures, since there were not enough data to derive Arrhenius kinetic constants. The initial concentrations of total iron ions = 0.02 ppm and tocopherols = 165 ppm (Hoppenreijs et al., 2021). Initial concentrations of oxidation products were collected from experimental data at initial time. The standard deviations of the estimated kinetic constants (Eq. (21)) were <1%, indicating that the optimization is robust enough for the estimation of the constants. **f** are the estimated values of the acceleration factors to multiply with the kinetic constants during the second acceleration phase regarding Eq. (18). Only acceleration factors **f** greater than 1 are explicitly mentioned; otherwise they were equal to 1.

** $\mathbf{k}_{EP} = \mathbf{k}_{e1}\mathbf{k}_{e2}$ (Eq. (7)) and $\mathbf{k}_{EPOOH} = \mathbf{k}_{e1}\mathbf{k}_{e2}\mathbf{k}_{e3}$ (Eq. (8)).

\# Reported literature values were not specified per type of fatty acids. Kinetic constants $\mathbf{k}_i$, $\mathbf{k}_{p2}$, and $\mathbf{k}_d$ were previously reported in (Takahashi et al., 2021)[a], $\mathbf{k}_{p2}$ and, $\mathbf{k}_{p1}$ in (Niki et al., 1993)[b], and $\mathbf{k}_a$ and $\mathbf{k}_{EP}$ in (St. Angelo, 1992)[c].

where $[O_{2,S}]$ (in $mol.m^{-3}$) designates the O_2 concentration at the headspace-oil surface and k_{H,O_2} is the O_2 solubility coefficient in oils (7.6×10^{-8} in $mol.m^{-3}.Pa^{-1}$ at 20 °C) (Cuvelier et al., 2017).

2.4.2.3. Modelling the second acceleration of lipid oxidation. As previously described, a second acceleration phase in lipid oxidation reactions is observed when the total LOOH concentration reaches a certain $C_{LOOH,\ critical}$ (Boerkamp et al., 2022; Merkx et al., 2021). This second acceleration phase was taken into consideration by including $\mathbf{k}_{CLOOH,\ critical}$ that is the vector of kinetic constants in Eqs. (1) to (17), when the $C_{LOOH,\ critical}$ was reached as:

$$\mathbf{k}_{CLOOH,critical} = \mathbf{f} \times \mathbf{k} = f(1) \times k(1) + f(2) \times k(2) + f(3) \times k(3) \quad (18)$$

where **f** = (f(1), f(2), f(3)) represents the vector of the multiplication factors (unitless) originating from fatty acids with 1-, 2- and 3- double bonds, respectively.

2.4.2.4. Optimization of the model parameters. The final mechanistic kinetic model was built using Eqs. (1) to (18). Model parameters including the initial concentrations of fatty acids, oxidation products, iron ions, tocopherols, and vial dimensions were collected from experiments (Boerkamp et al., 2022). However, for solving the governing equations (Eqs. (1) to (18)) of the final model, the unknown parameters k_{Pe}, **k**, $C_{LOOH,\ critical}$ and **f** need to be determined. The value of k_{Pe} was estimated by fitting the increase in O_2 partial pressure (in %) over time in nitrogen-flushed vials incubated at 20 and 40 °C. After fixing the k_{Pe} value, the remaining parameters **k**, $C_{LOOH,\ critical}$ and **f** were estimated by fitting the training dataset at 20 and 40 °C under the limited O_2 condition. The fitted curves (X) were the O_2 partial pressure (in %) in the headspace (Eq. (12)) and the concentrations over time of LOOHs, ADs, and EPs (in $mmol.kg^{-1}$ oil) in Eqs. (1) to (11). To simultaneously fit the curves X with the multiple experimental results, we employed a multi-response optimization (van Boekel, 2008). The multi-response optimization was conducted using Matlab R2021b software (Mathworks, Natick, MA, USA). The '*ode15s*' solver was employed to numerically solve the governing equations (Eqs. (1) to (17)) with variable time steps, where the default tolerances were adjusted to obtain accurate numerical solutions. Then, the '*lsqnonlin*' algorithm was employed to find **k**, $C_{LOOH,\ critical}$ and **f** by minimizing the sum of the squared errors between the experimental and numerical datasets. Since each squared error was in different value scales, the experimental and numerical datasets ($\widetilde{X}$) were normalized following Eq. (19) before calculating the sum of squared errors (Eq. (20)):

$$\widetilde{X} = \frac{X - \min(X_{exp})}{\max(X_{exp}) - \min(X_{exp})} \quad (19)$$

where subscripts exp embodies experimental kinetic curves X.

$$\|\widetilde{X}_{exp} - \widetilde{X}_{num}\|_2^2 = \sum_{i=1}^{n_t} \left(\widetilde{X}(t_i)_{exp} - \widetilde{X}(t_i)_{num}\right)^2 \quad (20)$$

where t, i, and n_t indicate storage time, index of time points, and the total number of time points, respectively.

After fitting the normalized numerical and experimental datasets, the precision of these estimated values was evaluated using Monte Carlo simulations with 200 iterations to calculate the standard deviation (van Boekel, 2008):

$$X_{noise,exp} = X_{exp} + \sigma r_1 r_2 \quad (21)$$

where X_{noise} and X_{exp} are the noised and original experimental data, respectively, σ is the experimental standard deviation estimated for each experimental data, and r_1 and r_2 are random values varying from 0 to 1. The computational simulations were run on a computer having 2.60 GHz, x64-based processor with 32 GB of RAM.

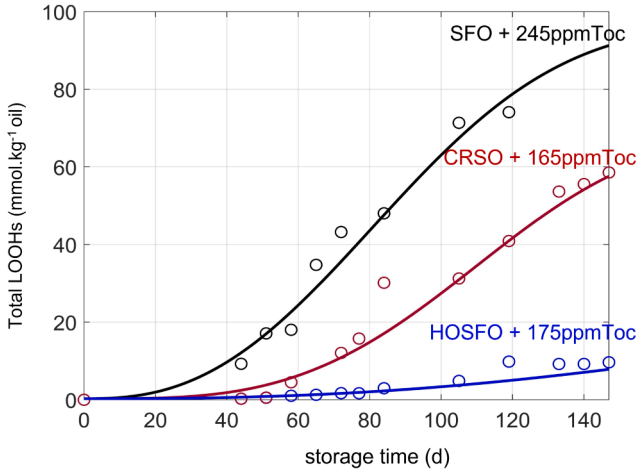

Fig. 2. Model predictions (lines) and experimental results (open circles) for total hydroperoxides in oils under initial 21% O_2 headspace in closed containers. The three oils were sunflower oil with 245 ppm tocopherols (black line and circles, SFO + 245 ppm Toc), conventional rapeseed oil with 165 ppm tocopherols (dark red line and circles, CRSO + 165 ppm Toc), and high-oleic sunflower oil with 175 ppm tocopherols (blue line and circles, HOSFO + 175 ppm Toc). (For interpretation of the references to colour in this figure legend, the reader is referred to the web version of this article.)

2.4.3. *Evaluating the prediction model*

After building the final model and estimating its parameters, its ability to predict the formation of oxidation products (i.e., LOOHs, aldehydes, and epoxides) in oils with different composition and/or stored under various O_2 conditions, as well as from a limited early oxidation dataset was evaluated by comparing predicted curves with the test dataset (as summarized in Table S2). Due to the difference in value scales of the square errors between the experimental and numerical results, the normalized root mean square errors (NRMSEs) were used for this evaluation:

$$NRMSE = \sqrt{\frac{\sum_{i=1}^{n_t}\left(\widetilde{X}(t_i)_{predict} - \widetilde{X}(t_i)_{exp}\right)^2}{n_t}} \quad (22)$$

where $\widetilde{X}_{predict}$ and $\widetilde{X}_{exp}$ are the predicted kinetic curves and the experimental data points (with the normalization following Eq. (19), respectively.

First, the predictive capacity of the model was tested at different initial fatty acids and antioxidant composition as well as different O_2 conditions. In the kinetic modelling, the initial fatty acid (Eqs. (4) to (8)) and antioxidant (Eq. (9)) composition were changed by adjusting their initial amounts. Next, the O_2 conditions were changed by adjusting the initial % of O_2 partial pressure in the headspace in Eqs. (14) and (15). When under O_2 supply in open vials, there was an O_2 equilibrium between the headspace, external atmosphere, and oil, thus the kinetic rates for Eqs. (12) and (13) were equal to 0.

Ultimately, the final model estimated long-term LOOH formation and the formation of secondary oxidation products (aldehydes and epoxides) using short-time data collected before the $C_{LOOH,\ critical}$ was reached, to illustrate the possibility of reducing the required experimental time needed as reported in (Faubion et al., 2022). Here a short-time training dataset at 40 °C was used to estimate the kinetic constants of reactions related to antioxidants (R1-13 in Table 1), while all other parameters (e.g., **k**, $C_{LOOH,\ critical}$ and **f**) were kept the same estimated values as in section 2.4.2.4. The minimum time frame of the short-time dataset required for accurate extrapolations was also determined.

3. Results and discussion

3.1. *Contribution of O_2 mass transfers to lipid oxidation kinetics*

The O_2 mass transfer related to lipid oxidation is usually described by the decrease of the O_2 in the headspace (%) relative to the increase of oxidation products in the oil. Although our shelf-life studies were performed in tightly closed vials, the formation of oxidation products was still increasing, even when % O_2 consumption is very low and almost

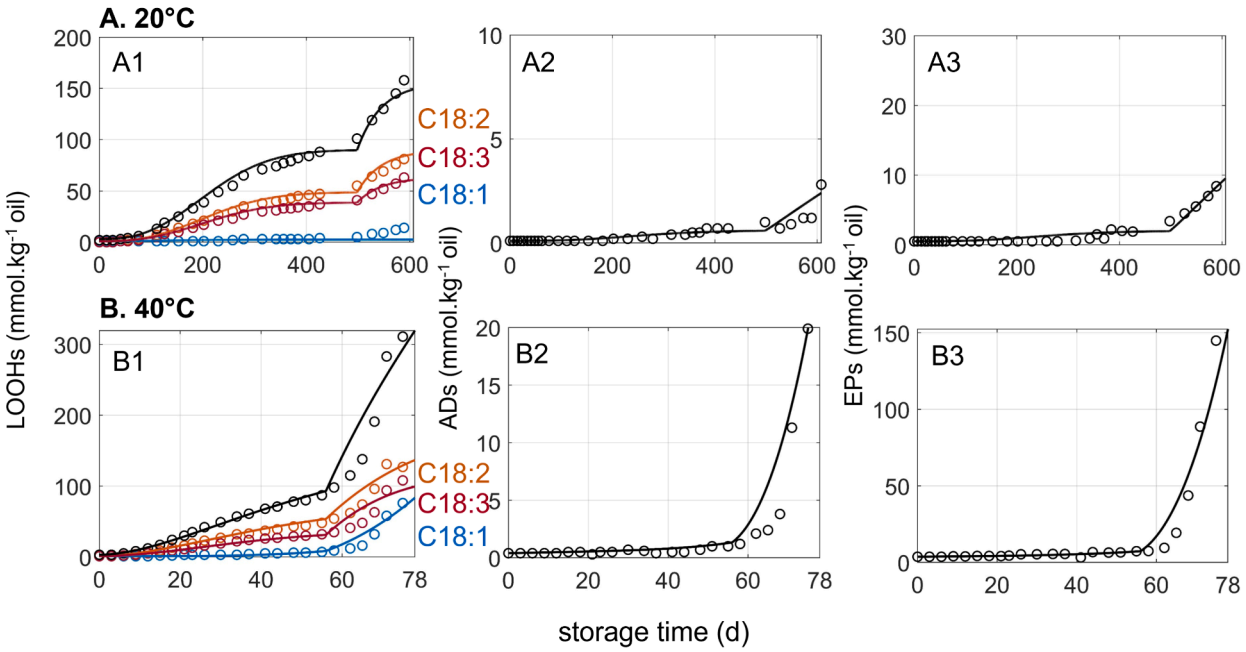

Fig. 3. Concentrations of oxidation products in non-stripped rapeseed oil predicted by the model (plain lines) versus the experimental data (open circles) at 20 and 40 °C. A1 and B1, concentration of total LOOHs from rapeseed oil (black) and specific LOOHs (coloured and labelled) derived from C18:1n-9, C18:2n-6, and C18:3n-3, A2 and B2 (concentration of total aldehydes), A3 and B3 (concentration of total epoxides) are data from the rapeseed oil.

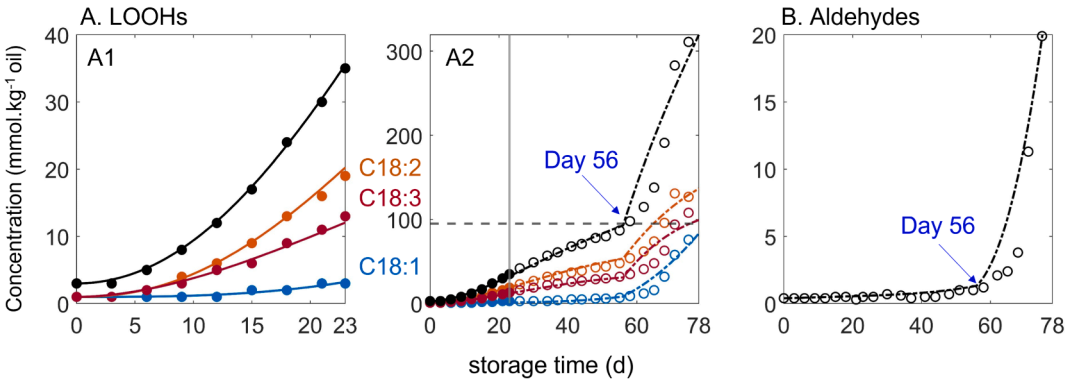

Fig. 4. The concentrations of LOOHs (A) and aldehydes (B) over time of rapeseed oil oxidized in open vials at 40 °C. A1, model fit (solid lines) with short-time experimental data of LOOHs (solid circles) for the first 23 days. A2, model extrapolation (dashed lines after the vertical gray line) compared to unused experimental datasets (empty circles). The horizontal dashed gray line indicates the $C_{LOOH,\ critical}$ of 95 mmol/kg oil. Note that the scale of the y axis between the sub-figures is different.

negligible after ~178 days at 20 °C and ~80 days at 40 °C (Fig. 1A1). These results suggested that O_2 was leaking through the cap, or in other words, that the cap used in the experiment allowed ingress of O_2 (Fig. S3). To experimentally determine the extent to which new O_2 entered the sample vials, experiments were performed using nitrogen-flushed vials with the same vial dimensions/conditions as our training datasets. These experiments showed that O_2 permeability and/or leakage through the cap was sufficient to replace 80% of the headspace over 100 days at 20 °C and 60 days at 40 °C (Fig. S4). This O_2 replacement countered loss of headspace O_2 by oxidation, so had to be accounted for in the model. Accordingly, experimental leakage data for each temperature was fit to (Eq. (14)) to calculate the kinetic constant k_{Pe}, yielding 1.5×10^{-15} and 2.12×10^{-15} (in $m^3.mol^{-1}.s^{-1}$) at 20 and 40 °C, respectively. When plugged into the final model, this seepage resulted in a net O_2 increase of around 7% at 20 °C and 5% at 40 °C (Figs. S5 and S6), providing important support for extended formation of oxidation products. These observations highlighted the importance of always determining potential O_2 ingress through the cap during shelf-life tests and, when warranted, including this parameter in the kinetic model via Eq. (14).

3.2. Estimation of the model parameters **k**, $C_{LOOH,\ critical}$, and **f**

The model parameters **k** (kinetic constants), $C_{LOOH,\ critical}$ (critical LOOH concentration), and **f** (acceleration factors) were estimated by simultaneously fitting the final mechanistic kinetic models (i.e., Eqs. (1) to (18)) with the training datasets, as illustrated in Fig. 1. The estimated kinetic constants before the second acceleration phase were in agreement with values previously reported in literature, when available (Table 2). The $C_{LOOH,\ critical}$ estimated by fitting the experimental data was 95 mmol/kg oil.

The acceleration factors **f** for all kinetic constants (Table 2) were determined from the training dataset at 40 °C, since the total LOOH concentration at 20 °C did not reach the $C_{LOOH,\ critical}$ (Fig. 1A2). Only kinetic constants, $\mathbf{k}_{p1}$, $\mathbf{k}_{p2}$, $\mathbf{k}_a$, and $\mathbf{k}_{EP}$ were accelerated, while the others remained constant. In future, when additional experimental data on e.g., radical concentrations are available, other kinetic constants might also need to be adjusted for the acceleration phase. In Table 2, the EPs had the highest acceleration factor (f_{kEP} of C18:3n-3 = 43.7), followed by ADs (f_{ka} of C18:2n-6 = 9.2), O_2 (f_{kp1} of C18:2n-6 = 6.1), and then LOOHs (f_{kp2} of C18:1n-9 = 2.93). To the best of our knowledge, this paper illustrates for the first time application of multiplication factors **f** to effectively describe the second acceleration phase in long-term incubations.

In this estimation, specific kinetic constants for each fatty acid types were used as described in section 2.4.2.1. The LOOH formation was faster for fatty acids with a higher number of double bonds and with a higher initial concentration, as shown in Fig. 1B. The formation of specific LOOHs was described well in the final model using the different kinetic constants estimated during optimisation (Table 2).

3.3. Use of $C_{LOOH,\ critical}$ and multiplication factors to describe the second acceleration phase

The formation of total LOOHs (Fig. 1A2) and different types of LOOHs (Fig. 1B1 and B2) were measured at 20 and 40 °C. At 20 °C, even after 294 days, the second acceleration was not observed, most likely because the total LOOH formation did not exceed the $C_{LOOH,\ critical}$ at this temperature. At 40 °C, once the $C_{LOOH,\ critical}$ was reached, the model correctly described the second acceleration phase when estimated values of multiplication factors (Table 1) were applied in Eq. (18). Use of multiplication factors accounted for increase in oxidation products with ~1.5 to 4.8 times (Fig. S7).

3.4. Evaluation of accuracy in model prediction

3.4.1. Oxidation prediction with different fatty acids and tocopherol concentrations

The final model (i.e., Eqs. (1) to (18)) developed from the training dataset of one oil was evaluated for its ability to simulate the LOOH formation of three other vegetable oils (test datasets 3–5 in Table S1) with different initial fatty acid compositions and initial tocopherol concentrations. This (test 1, Table S2) was accomplished by using three oils from which the dataset of the formation of total LOOHs was available- sunflower oil (SFO, 245 ppm tocopherols), conventional rapeseed oil (CRSO, 165 ppm tocopherols), and high-oleic sunflower oil (HOSFO, 175 ppm tocopherols). Because the same shelf-life conditions were used as the training test (40 °C with tocopherols under initial 21% O_2 headspace in closed containers), the same kinetic constants **k**, $C_{LOOH,critical}$, and **f** (Table 2) were applied to the final model to simulate the formation of total LOOHs in the three vegetable oils.

For each vegetable oil, based on the NRMSEs for all LOOHs formation (<0.1), the final model accurately simulated the formation of total LOOHs over time (Fig. 2), including detecting differences in oxidation due to oil composition (i.e., C18:1n-9, C18:2n-6, and C18:3n-3, and tocopherols). The concentration of aldehydes was not shown because it was below the limit of detection (<0.01 mmol/kg oil with ^{1}H NMR), and did not reach its onset time. This is also in line with the observation that LOOH formation did not exceed the $C_{LOOH,critical}$ of 95 mmol/kg oil. This test demonstrates that the final model design for LOOH prediction is

generalizable to multiple oil compositions.

3.4.2. Evaluation of the model prediction under different O_2 conditions

The ability of the final model, developed under initial 21% O_2 headspace in closed vials, to predict oxidation under different O_2 conditions was tested using non-stripped rapeseed oils oxidized in open vials (test datasets 1 and 2 in Table S1). This test (test 2 in Table S2) was performed using the final model (Eqs. (1) to (18)) in which the kinetic rates for Eqs. (12) and (13) were set to 0 (due to open vials) and the same model parameters **k**, $C_{LOOH,critical}$, and **f** as initially described (Table 2). The model predicted the formation of LOOHs, aldehydes, and epoxides in good agreement with the test datasets (Fig. 3), with NRMSEs between 0.04 and 0.02 and between 0.06 and 0.1, at 20 and 40 °C, respectively.

Using the kinetic values estimated from the training data (i.e., under initial 21% O_2 headspace in closed vials and taking into account the O_2 permeability/leakage through the cap) (Table 2), the model allowed us to predict the formation of oxidation products under a different O_2 condition (i.e., in fully open vials).

3.4.3. Evaluation of extrapolating short-time datasets of oils to estimate long-term formation of oxidation products at the same conditions in accelerated shelf-life tests

To access whether the model can successfully and accurately reduce experimental time of shelf-life testing, e.g., to compare effectiveness of different antioxidant levels or formulations, the model was used to extrapolate the short-time dataset from test dataset 2 (non-stripped rapeseed oils in open vials at 40 °C, Table S1). To accurately estimate long-term LOOH concentrations, a minimum timeframe of datasets including at least three data points from the onset of LOOH formation was needed (i.e., 23 days for the rapeseed oil in open vials at 40 °C).

Experimental LOOH concentrations from the first 23 days of rapeseed oil oxidation were fitted with the final model (i.e., Eqs. (1) to (18)) in which the kinetic rates for Eqs. (12) and (13) were set to 0 as the experiments were performed in open vials (Fig. 4A1). As the purpose of this test (test 3 in Table S2) was to evaluate the antioxidant activity, only the kinetic constants of tocopherols were estimated during the fitting procedure ($k_{AH1}(1) = 2.5\times10^{-2}$, $k_{AH1}(2) = 8.5\times10^{-3}$, $k_{AH1}(3) = 8\times10^{-3}$; $k_{AH2}(1) = 1.7\times10^{-2}$, $k_{AH2}(2) = 7.8\times10^{-3}$, $k_{AH2}(3) = 8.4\times10^{-3}$), which were similar to those from fitting a whole time series in open vials (Table 2). The remaining parameters **k**, $C_{LOOH,critical}$, and **f** (Table 2) were kept at the same values in Table 2. These were used to estimate the full time series development of oxidation products under the same conditions, with acceptable NRMSEs (<0.1) in the data before reaching the $C_{LOOH,critical}$, and thereafter quantitatively good extrapolation.

The model extrapolation estimated a time of approximately 56 days to reach the $C_{LOOH,critical}$ (at the horizontal dashed line in Fig. 4A2) and the onset of aldehyde production (Fig. 4B), which is close to the experimentally measured time of around 60 days. Even after the $C_{LOOH,critical}$ point, the model predictions of LOOH and aldehyde formation show close accordance to the experimental data, although in this part the deviation from experimental data is larger than before the second acceleration phase. This accurate matching of predicted to actual data demonstrates that short-time LOOH datasets (e.g., <23 days) for oxidized oils are sufficient for the model to project long-term development of LOOHs and aldehydes. Further, the sample just given verifies that long-term antioxidant effectiveness can be predicted by incorporating estimated antioxidant kinetic constants into the model, then extrapolating early data points to predict when the $C_{LOOH,critical}$ was reached, determining the shelf-life. In this example, our model thus reduced the time required for shelf-life tests by around 41%.

4. Conclusion

A mechanistic kinetic model was developed to simulate the formation of lipid hydroperoxides, aldehydes, and epoxides in vegetable oils with different initial oil composition (i.e., different concentrations of oleic (C18:1n-9), linoleic (C18:2n-6), and alpha-linolenic (C18:3n-3) acids and tocopherols) at 20 and 40 °C, and under different O_2 conditions. We realise that in reality, there could be others differences in oil composition: UFA composition, the amount and type of antioxidants and prooxidants. It is therefore necessary to extend the model in future in order to apply it to these systems. The same is also true for the temperature effect on kinetic constants. The fast decomposition of LOOHs at high temperatures above 40 °C makes LOOHs ineffective as predictive markers to estimate the onset of secondary oxidation products. Tests of applications will show if and how the extended model should be modified to accurately predict oxidation in a wide range of materials.

This study thus shows an approach to come to a mechanistic kinetic model that in future may be extended to allow application for more complex oxidation systems and conditions, such as foods and emulsions. The model encompassed detailed steps and reactions involved in the progression of lipid oxidation, including O_2 consumption in headspace and formation of LOOHs, aldehydes, and epoxides that are important determinants of oil stability and shelf life. The final model was obtained by describing underlying lipid oxidation reactions and by accounting for all O_2 mass transfer processes in the system. For completeness and accuracy, the final model incorporated specific kinetic constants of reactions related to specific unsaturated fatty acids as well as acceleration factors for adequately describing the second acceleration phase of lipid oxidation reactions after a critical hydroperoxide concentration is reached. Multi-response optimization used training oxidation data from oxidized commercial rapeseed oil in closed vials with O_2 permeability/leakage through cap at 20 and 40 °C to estimate the model parameters once. The generalizability of this final model was then demonstrated in its ability to accurately simulate the formation of oxidation products in rapeseed oils under a different O_2 condition (in fully open vials) at 20 and 40 °C, as well as in three other oils with different unsaturated fatty acid and tocopherol compositions in open vials at 40 °C.

Most importantly, the model could well extrapolate the onset of aldehydes, from a limited number of data points (at least three after LOOH begins to form) measured early in oxidation, thus estimating shelf-life. This can reduce the amount of experimental time required for shelf-life testing time by several months.

CRediT authorship contribution statement

Khoa A. Nguyen: Conceptualization, Methodology, Software, Investigation, Formal analysis, Validation, Writing – original draft. **Marie Hennebelle:** Conceptualization, Supervision, Writing – review & editing. **John P.M. van Duynhoven:** Conceptualization, Supervision, Writing – review & editing, Funding acquisition. **Arend Dubbelboer:** Conceptualization, Supervision, Writing – review & editing. **Vincent J. P. Boerkamp:** Conceptualization, Formal analysis, Investigation, Writing – review & editing. **Peter A. Wierenga:** Conceptualization, Supervision, Writing – review & editing, Funding acquisition.

Declaration of Competing Interest

The authors declare that they have no known competing financial interests or personal relationships that could have appeared to influence the work reported in this paper.

Data availability

Data will be made available only on request.

Acknowledgements

We are grateful to Dr. Ewoud van Velzen (Unilever) for his expert advice on the kinetic modelling of lipid oxidation reactions. We thank Dr. Donny Merkx (Unilever) for his critical eyes on the chemical oxidation reactions to include in the model. This research received

funding from the Netherlands Organisation for Scientific Research (NWO) in the framework of the Innovation Fund for Chemistry (grant number 731.017. 301) and from the Ministry of Economic Affairs in the framework of the "TKI/PPS-Toeslagregeling".

Competing interests

The authors declare the following competing financial interest(s): Arend Dubbelboer and John P. M. van Duynhoven are employed by companies that manufacture and market oil based food products.

Appendix A. Supplementary data

Supplementary data to this article can be found online at https://doi.org/10.1016/j.foodchem.2023.137266.

References

Boerkamp, V. J. P., Merkx, D. W. H., Wang, J., Vincken, J.-P., Hennebelle, M., & van Duynhoven, J. P. M. (2022). Quantitative assessment of epoxide formation in oil and mayonnaise by 1H–13C HSQC NMR spectroscopy. *Food Chemistry, 390*(133145), 1–8. https://doi.org/10.1016/j.foodchem.2022.133145

Chaix, E., Broyart, B., Couvert, O., Guillaume, C., Gontard, N., & Guillard, V. (2015). Mechanistic model coupling gas exchange dynamics and Listeria monocytogenes growth in modified atmosphere packaging of non respiring food. *Food Microbiology, 51*, 192–205. https://doi.org/10.1016/j.fm.2015.05.017

Chen, B., Panya, A., McClements, D. J., & Decker, E. A. (2012). New insights into the role of iron in the promotion of lipid oxidation in bulk oils containing reverse micelles. *Journal of Agricultural and Food Chemistry, 60*, 3524–3532. https://doi.org/10.1021/jf300138h

Cuvelier, M.-E., Soto, P., Courtois, F., Broyart, B., & Bonazzi, C. (2017). Oxygen solubility measured in aqueous or oily media by a method using a non-invasive sensor. *Food Control, 73*, 1466–1473. https://doi.org/10.1016/j.foodcont.2016.11.008

Farhoosh, R. (2022). New insights into the kinetic and thermodynamic evaluations of lipid peroxidation. *Food Chemistry, 375*(131659), 1–10. https://doi.org/10.1016/j.foodchem.2021.131659

Farhoosh, R. (2021). Critical kinetic parameters and rate constants representing lipid peroxidation as affected by temperature. *Food Chemistry, 340*(128137), 1–8. https://doi.org/10.1016/j.foodchem.2020.128137

Faubion, N., David Pinkston, J., Schaich, K., Calligaris, S., Bolliet, D., & DellaPorta, R. (2022). Continuing the debate: Shelf life vs accelerated storage for evaluating antioxidants effectiveness. *INFORM magazine.*

Hoppenreijs, L. J. G., Berton-Carabin, C. C., Dubbelboer, A., & Hennebelle, M. (2021). Evaluation of oxygen partial pressure, temperature and stripping of antioxidants for accelerated shelf-life testing of oil blends using 1H NMR. *Food Research International, 147*(110555), 1–10. https://doi.org/10.1016/j.foodres.2021.110555

Johnson, D. R., & Decker, E. A. (2015). The role of oxygen in lipid oxidation reactions: A review. *Annual Review of Food Science and Technology, 6*, 171–190. https://doi.org/10.1146/annurev-food-022814-015532

Laguerre, M., Bily, A., Birtić, S., 2020a. Lipid oxidation in food, in: Lipids and edible oils. Elsevier, pp. 243–287. https://doi.org/10.1016/B978-0-12-817105-9.00007-0.

Laguerre, M., Bily, A., Roller, M., & Birtić, S. (2017). Mass transport phenomena in lipid oxidation and antioxidation. *Annual Review of Food Science and Technology, 8*, 391–411. https://doi.org/10.1146/annurev-food-030216-025812

Laguerre, M., Tenon, M., Bily, A., & Birtić, S. (2020b). Toward a spatiotemporal model of oxidation in lipid dispersions: A hypothesis-driven review. *European Journal of Lipid Science and Technology, 122*(1900209), 1–10. https://doi.org/10.1002/ejlt.201900209

Li, X., Wu, G., Huang, J., Zhang, H., Jin, Q., & Wang, X. (2020). Kinetic models to understand the coexistence of formation and decomposition of hydroperoxide during lipid oxidation. *Food Research International, 136*(109314), 1–9. https://doi.org/10.1016/j.foodres.2020.109314

Merkx, D. W. H., Hong, G. T. S., Ermacora, A., & Van Duynhoven, J. P. M. (2018). Rapid quantitative profiling of lipid oxidation products in a food emulsion by ^{1}H NMR. *Analytical Chemistry, 90*, 4863–4870. https://doi.org/10.1021/acs.analchem.8b00380

Merkx, D. W. H., Swager, A., van Velzen, E. J. J., van Duynhoven, J. P. M., & Hennebelle, M. (2021). Quantitative and predictive modelling of lipid oxidation in mayonnaise. *Antioxidants, 10*(287), 1–14. https://doi.org/10.3390/antiox10020287

Niki, E., Noguchi, N., & Gotoh, N. (1993). Dynamics of lipid peroxidation and its inhibition by antioxidants. *Biochemical Society Transactions, 21*, 313–317. https://doi.org/10.1042/bst0210313

Özilgen, S., & Özilgen, M. (1990). Kinetic model of lipid oxidation in foods. *Journal of Food Science, 55*, 498. https://doi.org/10.1111/j.1365-2621.1990.tb06795.x

Patsioura, A., Ziaiifar, A. M., Smith, P., Menzel, A., & Vitrac, O. (2017). Effects of oxygenation and process conditions on thermo-oxidation of oil during deep-frying. *Food and Bioproducts Processing, 101*, 84–99. https://doi.org/10.1016/j.fbp.2016.10.009

Pénicaud, C., Guilbert, S., Peyron, S., Gontard, N., & Guillard, V. (2010). Oxygen transfer in foods using oxygen luminescence sensors: Influence of oxygen partial pressure and food nature and composition. *Food Chemistry, 123*, 1275–1281. https://doi.org/10.1016/j.foodchem.2010.05.065

Schaich, K.M., 2020. Lipid oxidation: New perspectives on an old reaction, in: Shahidi, F. (Ed.), Bailey's industrial oil and fat products. Wiley, pp. 1–72. https://doi.org/10.1002/047167849X.bio067.pub2.

Schneider, C., Boeglin, W. E., Yin, H., Porter, N. A., & Brash, A. R. (2008). Intermolecular peroxyl radical reactions during autoxidation of hydroxy and hydroperoxy arachidonic acids generate a novel series of epoxidized products. *Chemical Research in Toxicology, 21*, 895–903. https://doi.org/10.1021/tx700357u

Syed, A., 2016. Oxidative stability and shelf life of vegetable oils, in: Oxidative stability and shelf life of foods containing oils and fats. Elsevier, pp. 187–207. https://doi.org/10.1016/B978-1-63067-056-6.00004-5.

Takahashi, A., Suzuki, J., Shibasaki-Kitakawa, N., & Yonemoto, T. (2001). A kinetic model for co-oxidation of β-carotene with oleic acid. *Journal of the American Oil Chemists' Society, 78*, 1203–1207. https://doi.org/10.1007/s11745-001-0414-9

Takahashi, A., Takahashi, R., Hiromori, K., & Shibasaki-Kitakawa, N. (2021). Quantitative evaluation of oxidative stability of biomembrane lipids in the presence of vitamin E. *Journal of the American Oil Chemists' Society, 98*, 567–579. https://doi.org/10.1002/aocs.12480

van Boekel, M.A.J.S., 2008. Multiresponse kinetic modeling of chemical reactions, in: Kinetic modeling of reactions in foods, 0 ed. CRC Press, pp 1-32. https://doi.org/10.1201/9781420017410.

Wardhani, D. H., Fuciños, P., Vázquez, J. A., & Pandiella, S. S. (2013). Inhibition kinetics of lipid oxidation of model foods by using antioxidant extract of fermented soybeans. *Food Chemistry, 139*, 837–844. https://doi.org/10.1016/j.foodchem.2013.01.049